KSCE Journal of Civil Engineering (2021) 25(3):782-792
DOI 10.1007/s12205-021-0161-3

pISSN 1226-7988, eISSN 1976-3808
www.springer.com/12205

Geotechnical Engineering

Internal Force of the Anti-slide Pile in Soil Based on the Deep Beam Model

Jun Wang[a], **Jie Liu**[a,b], **and Qiao Liang**[a]

[a]*Dept. of Building Engineering, Hunan Institute of Engineering, Xiangtan 411104, China*
[b]*School of Resource Environment and Safety Engineering, Hunan University of Science and Technology, Xiangtan 411201, China*

ARTICLE HISTORY

Received 28 January 2020
Revised 20 May 2020
Accepted 15 June 2020
Published Online 22 January 2021

KEYWORDS

Anti-slide pile
Bearing characteristics
Calculation model
Internal force
Deep beam theory

ABSTRACT

According to the deep beam model, the bury conditions, the geometry characteristics and the load condition, we established a load transfer model based on the tie rod arch and an internal force model for the loaded and anchored segments of the anti-slide pile. Then, we analyzed the shear, bending shear and local compressive failures of the pile, caused by the equivalent concentrated thrust force, the lateral frictional force, active earth pressure, and passive earth pressure, etc. With the laboratory results of the deep beam model, the relation between the shear span ratio and the tie rod arch was presented. According to the mechanical balance conditions of the cantilever beam, we obtained the power function curve of the tie rod arch and the influence factors. Subsequently, we established the equations of the horizontal displacement and the deflection angle at the bearing segment by superposing the load and the displacement of the strip nodes. According to the deformation characteristics of the Timoshenko deep beam element, the equations of the horizontal displacement and the deflection angle at the anchored segment were proposed. With the established calculation model and the material mechanics, the displacement, shear force and bending moment curves at the loaded and anchored segment of the anti-slide pile were proposed. Finally, the case study indicates that the displacement and the internal forces are nonlinear in the pile. The results obtained using the preliminary beam are larger than the numerical results, which is the smallest results than the other two methods.

1. Introduction

Anti-slide piles, bearing horizontal forces, have been widely used to support slopes and lateral wall of the caverns. The concrete at the anchored segment (bottom segment), the resistance of the surrounding soil and the improvement of the sliding body can resist the thrust from the upper segment of the pile, and reinforce the pile-soil structure (Kahyaoglu et al., 2012; Wang et al., 2017). Extensive studies have investigated the distribution, geometry design, internal force and parameter optimization of the anti-slide pile. Frequently, the pile geometries are determined by engineering practices and design code, based on many assumptions and the preliminary beam model. The structure-load, Poulos, Ito Tomio and Viggani methods can be used to theoretically calculate many mechanical parameters of the anti-slide pile, including slide force, anti-slide force, safety factor of stability, shear stress, bending moment and displacement, etc. Extensive practical studies show that piles frequently fail because of the large deformation or the insufficient strength of the loaded segment.

To facilitate the corresponding study, the load transition mode, the anti-slide mechanism and the internal forces have been investigated, based on the simplified cantilever model and the elastic foundation beam model. In addition, in the calculation process, the plane cross-section assumption has been adopted. Subsequently, by adopting the material mechanics and the preliminary beam theory, extensive previous studies significantly contribute to obtaining the bending moment, shear stress and internal forces of the anti-slide pile (Zhao et al., 2017; Zhao et al., 2018). Dai and Shen (2003) first obtained the distance between the slide surface and the turning point, and the deflection angle at the slide surface. Then, they calculated the

CORRESPONDENCE Jun Wang 277210509@qq.com Dept. of Building Engineering, Hunan Institute of Engineering, Xiangtan 411104, China

bending moment and the shear stress of the pile, using the m method. Yin et al. (2017) investigated the internal force and the displacement of the cable pile, based on the deformation characteristics of the shallow pile and the deformation coordination of the pile anchored body. Kourkoulis et al. (2011) first calculated the slide force and the slope pressure distribution, by analyzing the displacement of the surrounding soil. They further obtained the internal force by assuming the anti-slide segment as an indeterminate structure. Matsui and San (1992) monitored the deformation, shear stress and bending moment of the field anti-slide piles. Subsequently, they optimized the design parameters according to the field tests and the theoretical calculations. Wang and Zhang (2014) investigated the influence of the length of the pile on the displacement and internal stress distribution, by simulating the shallow elastic beam.

The above studies significantly contribute to understanding the reaction mechanism of anti-slide piles to the slide force. In previous studies, homogeneous bending deformation occurred in the axially symmetric piles. However, the effects of the frictional forces on the lateral surface and the bearing surface, the weight of the pile, the shear strain on the horizontal section and the nonlinear deformation on the displacement and internal stress of the pile lack sufficient studies.

The interaction between the anti-slide pile and soil is very complicated, because the inhomogeneous loads on the pile result from the slide force, the resist force of the soil, the tension force of the cable or bolt, the weight of the pile and the lateral and bottom frictional forces. The theoretical solution of the internal force today based on the deep beam theory instead of the preliminary beam theory may be more accurate, because of the large cross section and inhomogeneous loads. According to the GB 50010-2010, the span-height ratio of the medium-deep beam ranges from 2 to 2.5. The code fails to define the cantilever, bearing shear stresses and frictional forces. Practically, significant shear stresses and frictional forces may result from the slide force, resist force and lateral friction. Recent, Lei et al. (2013) considered the frictional forces and proposed that the critical displacement and the residual shear strength may significantly affect the displacement and internal stress of the pile. However, they ignored the inhomogeneous deformation. Thus, the load transition mode, the curve equation and the load distribution of the tied arch, the inhomogeneous deformation and the calculation of the internal force deserve further investigations.

In the present article, we simplified the slide force into concentrated load, according to the loading conditions and geometry size of the pile. Then, we established a deep beam model, considering the intensity of the frictional force and the earth pressure, to study the bearing characteristics and internal forces. Subsequently, the reasonability of this model and the discrepancy between the proposed model and the preliminary model were investigated.

2. The Bearing Characteristics and the Failure Pattern of the Deep Pile

2.1 The Structure and the Load Conditions of the Anti-slide Pile

Shear failure may occur in slopes, caverns and foundations as

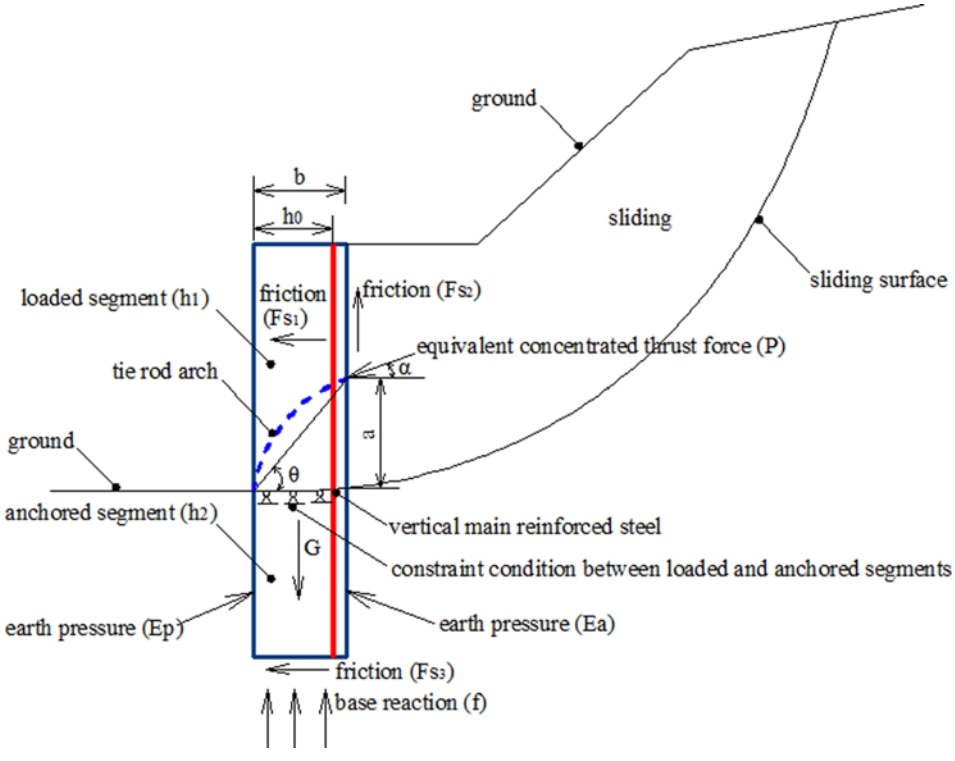

Fig. 1. Structure and Loading Conditions of the Anti-sliding Pile

shear force exceeds the shear strength of the soil. Anti-slide piles, an important supporting structure, can properly resist shear slide. According to the failure characteristics, the anti-slide pile consists of the loaded segment (the segment above the slide surface) and the anchored segment (the segment beneath the slide surface). Additionally, the bearing force, the deformation and the failure pattern of these segments may vary because of the differences in boundary conditions. Without considering the passive soil pressure, the loaded segment and the anchored segment can be treated as a cantilever and an elastic foundation beam.

Recent, the anti-slide piles have been simplified into preliminary beam structures. In the calculation of the internal force and pile parameters, the effects of the horizontal thrust at the loaded segment and the earth pressure at the anchored segment on the internal forces are investigated. Practically, the pile structure is a coupled bearing system, affected by the soil layers condition. The anti-slide pile may slide, rotate and bend under load. Simultaneously, the earth pressure and the anti-slide force may continuously adjust. With the perimeter frictional force and the gravity load of the pile (Fig. 1), the deformation and the stability of the pile may be significantly affected.

$F_{si}(i=1,2,3)$ is the frictional force, written as

$$F_{si} = \int_0^A q_{si} dA \,, \tag{1}$$

where A and q_{si} are the frictional area and the frictional intensity, respectively.

2.2 Load Bearing Characteristics

2.2.1 Arch Curve of the Tie Rod

The loaded segment, directly contacting with the slide body, may submit because of the residual slide thrust. To analyze the effect of thrust on the pile deformation and the internal force, the distribution thrust force was equivalent to the concentrated thrust, P. Referring to the regulation (GB 50010-2010) and the definition on the shear span ratio of the deep beam element (Li et al., 2018), we simplified the anti-slide pile into the deep beam model:

$$\lambda = \frac{\sum M}{Qh_0} = \frac{(P \cdot a \cdot \cos\alpha + F_{s1} \cdot l + F_{s2} \cdot b - P \cdot b \cdot \sin\alpha)}{(P\cos\alpha + F_{s1}) \cdot h_0} \,, \tag{2}$$

where λ, Q, P, M, h_0, a, l, b and α are the shear span ratio, the shear stress, the concentrated load, the bending moment, the effective height, the distance between the concentrated load and the base, the distance between the frictional surface and slide face, the width of the anti-slide pile and the angle determined by the equivalent concentrated thrust and horizontal direction.

Equation (2) shows that the shear span ratio is equal to $\frac{a}{h_0}$ which satisfies the conditions for the preliminary beam without considering the lateral friction force, F_{s1}. Thus, the reasonability of Eq. (2) is verified. The thickness distribution of the sliding body and the mechanical monitor results indicate that the distance between the location of the equivalent concentration thrust force, P, and the slide surface is about (1/4 – 1/3)h1. With the minimum design width of 1.25, we can infer that the shear span ratio ranges from 1 to 5. Thus, shear pressure and inclined tensile failures occur (Xia and Zeng, 2015). The preliminary beam theory indicates that bending failure on the normal section, the compressive failure on the inclined section, the shear pressure failure and the inclined tensile failure may occur (Brandenberg et al., 2005; Li et al., 2015).

Actually, the anti-slide pile is a deep beam instead of a preliminary shallow beam because of the structural sizes, the deformation characteristics and the load condition. Additionally, stress redistributions occur before the pile fails. Thus, the sectional deformation is non-planar. Simultaneously, shear failure, bending failure and local compressive failure at the upper part of the anchorage segment occur. Therefore, we adopted deep beam theory to study the bearing characteristics and the failure patterns of the anti-slide pile. The load loaded and anchored segments are treated as deep beams. An arch-shaped load transfer model forms (Fu and Zhang, 1992). With the load distribution in Fig. 1, we can establish a tie rod arch model with variable sections (Fig. 2), consisting of the concrete (the inclined compressive bar) and the steel bar (the tension bar).

Stress redistributions occur in the beam when cracks at the loaded segment form. The soffit concrete fails because of the compression. Then, the further crack development results in the shear failure. Thus, the shear span ratio significantly affects the curvature of the arch and the final failure pattern. According to the load transfer model and previous results (Fu and Zhang, 1992), Fig. 3 shows the curve of the shear span ratio and the diagonal inclination angle of the tie rod arch.

The fitting power function equation is

$$\lambda = m47.017\theta^{-0.8453n} \,, \tag{3}$$

where m and n are experimental constants, λ and θ are the shear span ratio and diagonal inclination angle, respectively.

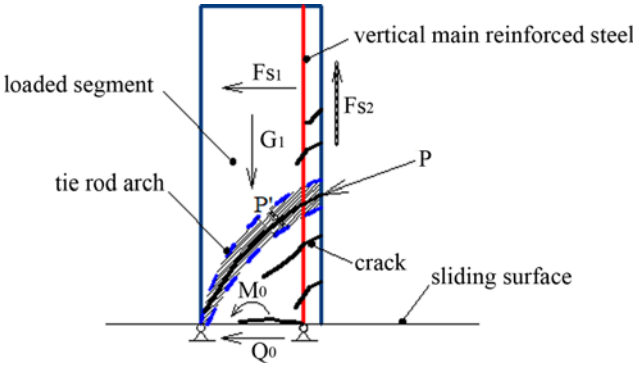

Fig. 2. Transmission Mode and Destruction Pattern (Q_0, M_0, F_{s1}, F_{s2}, P and G_{s1} are the shear force on the sliding surface, the bending moment on the sliding surface, the lateral friction force, the lateral frictional force at the bearing segment, the concentrated thrust and the gravity load of the bearing segment, respectively.)

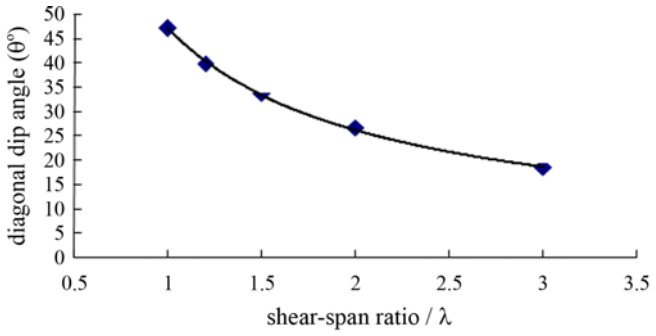

Fig. 3. Relation Between Shear-Span Ratio and Diagonal Dip Angle of Arch

Clearly, the shear span ratio decreases the diagonal dip angle (α in Fig. 1). In addition, the decrease rate slightly decreases with the increase in the shear span ratio. The larger variation in the arch curvature affects the shear strength more significantly.

2.2.2 Residual Slide Force

In the preliminary beam model, residual force, frequently causing pile deformation, can be calculated using the elastic foundation model. In the deep beam model, we can calculate the residual force based on the shear elastic model using the Timoshenko deep beam element (Xia and Zeng, 2016). Considering the subgrade reaction and the foundation deformation in the reversed direction, the residual slide force along the loaded segment is

$$P(x) = ky(x) - G_s \frac{d^2 y(x)}{dx^2} + 2\int_{h_2}^{h_1+h_2} F_{s1} b dx - 2\int_{0}^{h_2} F_{s5} b dx - F_{s3}, \quad (4)$$

where k, $y(x)$, G_s, F_{s5}, F_{s3} and b are the stiffness, the displacement of the pile body, the shear stiffness of the soil, the frictional force on the lateral surface of the anchored segment, the bottom frictional force and width of the bearing surface, respectively. h1 and h2 are the lengths of the loaded and anchored segments.

The increase of the deformation at the loaded segment may increase the residual slide force. At the top part of the pile, the residual force is relatively high, whereas the residual force near the slide surface is much lower. Simultaneously, the lateral friction force may also affect the residual slide force. However, previous studies frequently ignored the lateral friction force. Thus, the corresponding results are relatively conservative.

2.3 The Bearing Characteristics at the Anchored Segment

To ensure the stability of the anti-slide structure and restrain slide deformation, a part of the pile (the anchored segment) is frequently embedded in the stable soil or rock. The design anchor depth may vary with the change in soil or rock properties. For the soil or the soft rock, the anchor depth ranges from 1/3 times to 1/2 times of the pile length. For the hard rock, the anchor depth decreases to 1/4 times of the pile length. The shear force and bending moment on the slide surface, the passive earth pressure ahead the pile, the active earth pressure behind the pile,

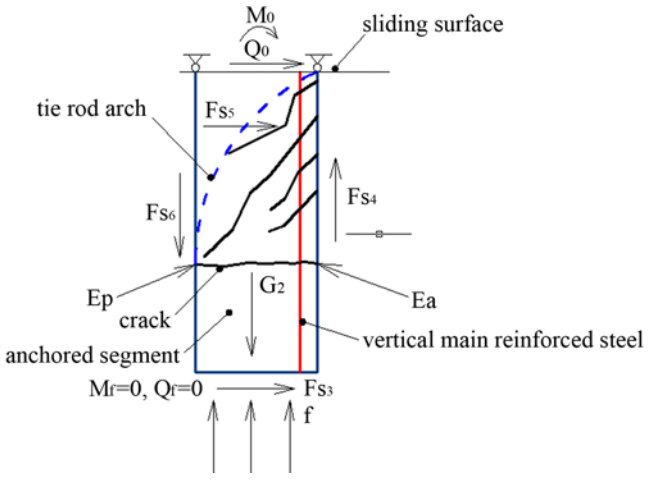

Fig. 4. Load Transfer Mode and Failure Pattern at the Anchored Segment

the lateral friction force, the base counter-force and the gravity load may act on the anchored segment. In the present article, the pile locates in soils, thus, the pile bottom is free. Then, with the geometric characteristics and load conditions, the anchored segment can be treated as a deep beam element (Fig. 4).

Various forces, including the passive earth pressure, E_p, the friction force on the compression surface, F_{s4}, the base counter-force, f, and the gravity load, G_2, may highly compress the anchored segment. Then, the concrete may fail because of the crack development, resulting from compression. Thus, local failure at the point where the passive pressure acts on may occur. Simultaneously, the relatively large stress and strain increments and stress concentrations on the slide surface, the concrete may fail because of the extensive tensile-shear cracks. Subsequently, bending shear failures may occur with further crack development at the arch concrete. The slide surface may restrain this failure zone, thus, a tie rod mode, characterized by the inclined compression rod and the tensile steel bar, forms (Fig. 4).

3. The Calculation Model and the Control Equation of the Anti-slide Beam Pile

3.1 Calculation Model

Presently, the internal forces and the design parameters at the loaded and anchored segments are obtained based on the preliminary beam theory and the elastic foundation beam model. First, the displacement and the internal variables are obtained by analyzing the geometric structure, the physical parameters of the material and the load conditions. Then, the shear force and the bending moment are calculated. Subsequently, the shear force and the internal bending force can be obtained (Liu and Wang, 2018). However, the field and laboratory tests reveal that the deformation and the internal force, especially the shear force and the pile axis, are uneven on the cross section. In addition, the displacement at the top is relatively higher and decreases along

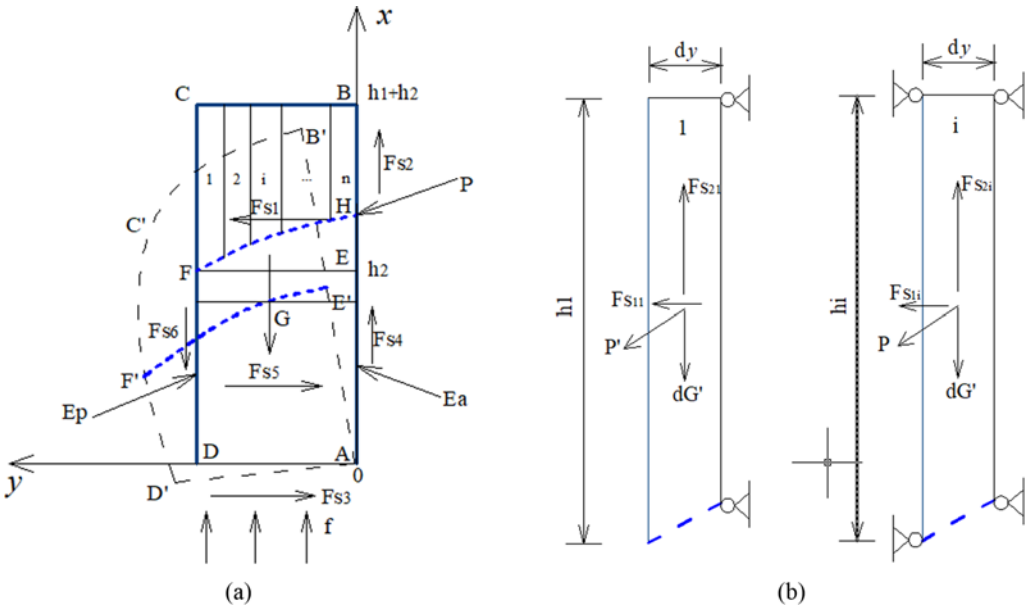

Fig. 5. Calculation Model: (a) Deep Beam Model, (b) The Internal Force between Strips

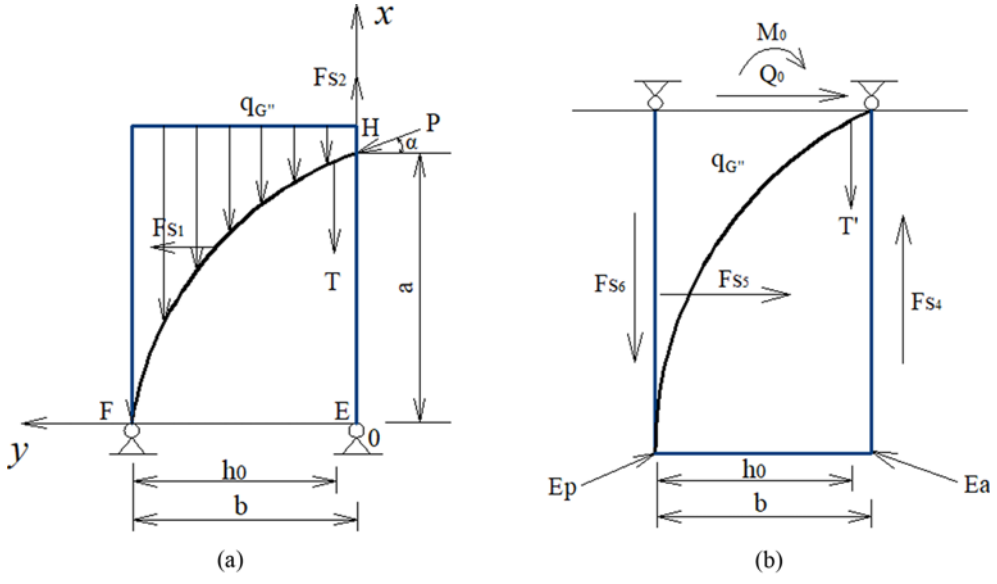

Fig. 6. Calculation Model of the Tie Rod Arch: (a) Calculation Model of the Bearing Segment, (b) Calculation Model of the Anchored Segment (T, h_0, q_C, F_{s1} and F_{s2} are the tensile force, the effective height, the gravity concentration, the lateral friction force and the friction force behind the pile, respectively.)

the pile length. Moreover, the pile axis and the pile boundary are uneven curves. Thus, the deep beam under shear is more proper (Fig. 5).

Displacement of the pile along the slide direction may occur, under the slide driving force. The restraint of the tie rod arch may result in the relatively larger deformation and force at the upper part of the loaded segment. In the present article, vertical strip method is applied because the plane section assumption is infeasible. The pile deformation can be obtained by superposing the element displacements (Fig. 5).

3.2 The Equation for the Tie Rod Arch

The arch consists of the inclined compression rod and the tensile steel bar (Fig. 6). The deformation of the arch at the loaded segment is much higher than that at the anchored segment. In the present article, we mainly investigate the arch characteristics at the loaded segment.

The loads on the tie rod arch mainly includes the tensile force, the effective height, the gravity concentration, the lateral friction force and the friction force behind the pile (Fig. 6). A hinged connection forms on the slide surface. According to the equilibrium conditions and Eq. (1), the horizontal and vertical forces at the loaded segment are

$$F_x = \int_0^b q_{s2}(h_1 - x)dy - \int_0^b \gamma_s dy - T - P\sin\alpha \,, \tag{5}$$

$$F_y = \int_0^a q_{s1}(b - y)dx + P\cos\alpha \,, \tag{6}$$

where γ_s, q_{s1}, q_{s2} and P are the unit weight of soil, the concentrated lateral friction force at the loaded segment, the concentrated lateral friction force behind the pile and the equivalent thrust, respectively.

The bending moment at the centroid of the slide surface EF is

$$M(y) = \begin{cases} [\int_y^b \gamma_s(a-x)dy]\cdot\left(\dfrac{b-y}{2}\right) & \dfrac{1}{2}b < y \le b \\ [\int_0^y \gamma_s(a-x)dy]\cdot\dfrac{1}{2}y + T(b-h_0) - \int_0^{\frac{1}{2}y} q_{s1}(a-x)dy]\cdot\dfrac{1}{2}y & 0 < y \le \dfrac{1}{2}b. \end{cases} \tag{7}$$

According to the displacement at the slide surface and the continuous distribution of the bending moment, Eq. (7) yields

$$M(y)_{-\frac{1}{2}b} = M(y)_{\frac{1}{2}b} \,. \tag{8}$$

Then, the tension of the main steel bar, T, is

$$T = \frac{b^2 q_{s1}}{16(b-h_0)} \,. \tag{9}$$

The tie rod arch fails when the bending moment is high enough. The corresponding maximum and minimum bending moments are

$$M'(y) = \begin{cases} \dfrac{1}{2}\gamma_s(a-x)(b-y) & \dfrac{1}{2}b < y \le b \\ (\gamma_s - \dfrac{1}{2}q_{s1})(a-x)\cdot\dfrac{1}{2}y & 0 < y \le \dfrac{1}{2}b \end{cases} . \tag{10}$$

The A and B when the bending moments are the maximum or minimum are

$$\begin{aligned} &A(x_a = a, y_a = 0), \\ &B(x_b = 0, y_b = b). \end{aligned} \tag{11}$$

Equations (11) and (7) yield

$$M_{\min} = T(b - h_0) \,, \tag{12}$$

$$M_{\max} = ab\gamma_s + T(b-h_0) - \frac{1}{4}b^2 a q_{s1} \,. \tag{13}$$

Then, by incorporating Eq. (13) into Eq. (7), the arch equation is

$$y(x) = b - \sqrt{\frac{2[ab\lambda_s + T(b-h_0) - \frac{1}{4}b^2 a q_{s1}]}{\gamma_s(a-x)}} \,. \tag{14}$$

By introducing Eq. (9) into Eq. (14), the arch equation is

$$y(x) = b - \sqrt{\frac{abh_0\gamma_s + (q_{s1} - bh_0\gamma_s)x}{h_0\gamma_s b(a-x) + q_{s1}x} - 1} \,. \tag{15}$$
$$(0 \le x \le a, 0 \le y \le b)$$

Equation (15) shows that the increase in the shear span ratio increases the curvature of the arch, whereas the diagonal inclination angle of the tie rod arch decreases relatively rapid. This conclusion agrees well with the laboratory results (Fu and Zhang, 1992).

3.3 Deformation Calculation

3.3.1 Deformation at the Loaded Segment

Horizontal displacement and deflection may occur in pile because of the slide force, the earth pressure and the friction force. The loaded segment is a cantilever structure, thus, the deformation of the loaded segment is larger. Extensive field monitor results showed that the displacement on the cross section of the pile is dramatically uneven (Wang and Zhang, 2014). Thus, the deep beam model instead of the preliminary beam, using the plane assumption, is more appropriate for the calculation of the internal forces. To obtain the displacement of the loaded segment, the pile, treated as the deep concrete beam, is divided into several strips. The displacement of the loaded segment is expressed by the horizontal displacement and deflection (Fig. 5).

In the analysis process of the strips, the loads on the strip are equivalent to the nodal forces (Fig. 7). The superposition of the horizontal displacements, obtained using the material mechanics, can work out the deformation at one specific point.

According to the superposition principle, the horizontal displacement at a specific point is

$$\begin{aligned} w(x) &= \sum w_i(x) = w_{P_y}(x) + w_{Fs1}(x) + w_{M_{Py}}(x) + w_{Px}(x) - w_{Ms1}(x) - w_{Ms2}(x) \\ &\frac{P\sin\alpha}{6EI}x^2(3h_1 - x) + \frac{(1-\frac{1}{b}y)q_{s1}}{6EI}x^2(3h_1 - x) + \frac{P\sin\alpha}{2EI}(h_1 - a)x^2 \\ &+ \frac{P\sin\alpha}{6EI}x^2(3h_1 - x) - \frac{(1-\frac{1}{b}y)q_{s1}}{4EI}h_1x^2 - \frac{q_{s2}b^2}{4EI}h_1x^2 \\ &= \frac{2P\sin\alpha + (1-\frac{1}{b}y)q_{s1}}{6EI}x^2(3h_1 - x) + \frac{P\sin\alpha}{2EI}(h_1 - a)x^2 - \frac{(1-\frac{1}{b}y)q_{s1}q_{s2}b^2}{4EI}h_1x^2 \,. \end{aligned} \tag{16}$$

The deflection angle can be written as (Xu and Wu, 2007)

$$\theta = \frac{dw}{dx} \,. \tag{17}$$

Equations (16) and (17) yield

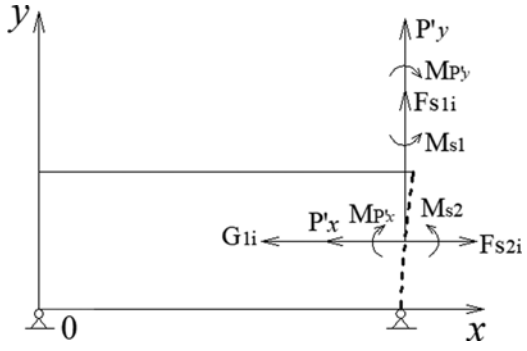

Fig. 7. Equivalent Endpoint Force (P_x, P_y, M_{px} and M_{py} are the equivalent horizontal and vertical concentrated thrusts and the corresponding moments; F_{s1}, F_{s2}, M_{s1} and M_{s2} are the friction forces and the corresponding moments.)

$$\theta(x) = -\frac{2P\sin\alpha + (1-\frac{1}{b}y)q_{s1}}{2EI}x^2 + 2[\frac{P\sin\alpha}{2EI}(h_1-a) + \frac{(1-\frac{1}{b}y)q_{s1}q_{s2}b^2h_1^2}{4EI} + \frac{2P\sin\alpha + (1-\frac{1}{b}y)q_{s1}}{2EI}h_1]x, \quad (18)$$

where EI is the anti-bending stiffness, qs1 and qs2 are the intensities of the friction force, a and θ are the angle determined by the equivalent thrust force and the horizontal plan, and the deflection angle, respectively.

Thus, many factors, especially the equivalent concentrated thrust force, the lateral friction force and the anti-bending stiffness, affect the pile deformation. Eq. (15) shows that the maximum deformation occurs at the external surface. In addition, the increase in the equivalent slide force increases the deformation, whereas the increase in the friction force decreases the deformation. Moreover, the gravity load hardly affects the deformation.

3.3.2 Deformation Calculation of the Anchored Segment

According to the load conditions at the anchored segment, the bending moment and shear force on the slide surface, the lateral friction force and the earth pressures ahead and behind the pile may significantly affect the deformation at the anchored segment. The displacement coordination between the soil and the pile before soil submit meets the requirement of the Winkler Foundation Theory, the internal force at the anchored segment can be calculated using the Timoshenko deep beam model. The deformation differential equation of the deep beam model is (Xia et al., 2010)

$$\begin{cases} \frac{d}{dx}[C(\frac{dw}{dx}-\theta)] - Kw = 0 \\ \frac{d}{dx}(D\frac{d\theta}{dx}) + C(\frac{dw}{dx}-\theta) = 0 \end{cases}, \quad (19)$$

where C is equal to $\frac{EA}{2\mu(1+\upsilon)}$, K, D, w, θ, E, υ and μ are the coefficient of subgrade reaction, the anti-bending stiffness, the horizontal displacement, the deflection angle, the elastic modulus of the pile, the Poisson's ratio and the shear modification coefficient, respectively.

Equation (19) yields

$$w(x) = e^{\beta\lambda x}\sin(\zeta\lambda x), \quad (20)$$

where $\lambda = \sqrt[4]{\frac{2\rho b E_S A(1+\upsilon_p)}{4EI[E_S A(1+\upsilon_p)+\mu El(1+\upsilon_s)}}$, $\mu = \frac{A}{I^2}\int_A \frac{S^2}{b^2}dA$,

$A = b\times l$, $\zeta = \sqrt{1-E\lambda^2[\frac{\mu I(1+\upsilon_s)}{E_s A}+\frac{1}{2\rho(1+\upsilon_p)}]}$,

$\beta = \sqrt{1+E\lambda^2[\frac{2\mu I(1+\upsilon_s)}{E_s A}+\frac{1}{2\rho(1+\upsilon_p)}]}$, $\rho = \frac{d\theta}{dx}$, μ, λ, S, υ_s, A

and ρ are the shear modification coefficient, the shear span ratio, the static moment of the pile, the Poisson's ratio of the soil, the sectional area of the pile and the curvature of the section, respectively.

The deflection angle is

$$\theta = \frac{dw}{dx} = \lambda e^{\beta\lambda x}[\zeta\cos(\zeta\lambda x) + \beta\sin(\zeta\lambda x)]. \quad (21)$$

Further, the curvature of the section is

$$\rho = \frac{d\theta}{dx} = \lambda^2 e^{\beta\lambda x}[2\beta\zeta\cos(\zeta\lambda x) - (\zeta^2-\beta^2)\sin(\zeta\lambda x)], \quad (22)$$

where φ the deflection angle of the pile axis.

According to the above analysis, we can infer that many factors, especially the anti-bending stiffness, the elastic parameters of the soil and the geometry size, significantly affect the deformation of the pile. In addition, the horizontal displacement, the deflection angle and the sectional curvature on the slide surface are larger. Similarly, the effect of the gravity load is negligible.

3.4 Calculation of the Internal Force

3.4.1 The Shear Force and Bending Moment at the Bearing Segment

Shear force and bending moment are two critical parameters for the anti-slide pile. Previous studies ignored the lateral friction force. Practically, the relative displacement between the soil, a frictional material, and the pile may cause non-negligible and uneven friction. In the present article, considering the lateral friction and the equivalent concentrated thrust force, the shear force is

$$Q(x) = \begin{cases} (1-\frac{1}{b}y)\cdot q_{s1}\cdot b\cdot(h_1-x) & 0\le y\le b,\ a<x\le h_1 \\ (1-\frac{1}{b}y)\cdot q_{s1}\cdot b\cdot(h_1-x)+P\cos\alpha & 0\le y\le b,\ 0<x\le a \end{cases}. \quad (23)$$

The integration of Eq. (23) yields

$$M(x) = (1-\frac{1}{b}y)\cdot q_{s1}\cdot b\cdot h_1^2 - \frac{1}{2}(1-\frac{1}{b}y)q_{s1}\cdot h_1^2 + Ph_1\cos\alpha + S \quad 0\le y\le b,\ 0\le x\le h_1-a. \quad (24)$$

When y is equal to 0, the bending moment is

$$M(x) = q_{s1}\cdot b\cdot(1-\frac{1}{b}y)\cdot(h_1-x) + \frac{1}{2}b^2\gamma_s(h_1-x) \quad 0\le y\le b,\ 0\le x\le a. \quad (25)$$

Equations (24), (25) and (26) yield ($x = 0, y = 0$)

$$S = \frac{1}{2}\gamma_s h_1 b^2 + q_{s1}h_1 b. \quad (26)$$

Then, substitute this value into Eq. (24), the bending moment

is

$$M(x)=\left(1-\frac{1}{b}y\right)\cdot q_{s1}\cdot b\cdot h_1^2-\frac{1}{2}\left(1-\frac{1}{b}y\right)q_{s1}\cdot h_1^2+Ph_1\cos\alpha+\frac{1}{2}\gamma_s h_1 b^2+q_{s1}h_1 b \quad 0\le y\le b,\ 0\le x\le h_1-a. \tag{27}$$

With the definite condition ($x=h_1, M(x)=0$), the bending moment at the loaded segment is

$$M(x)=q_{s1}\cdot b\cdot\left(1-\frac{1}{b}y\right)\cdot\left(h_1x-\frac{1}{2}x^2-\frac{1}{2}h_1^2\right) \quad 0\le y\le b,\ h_1-a<x\le h_1. \tag{28}$$

Equations (23) and (27) show that the distributions of the shear force and the bending moment along the pile are nonlinear. The maximum shear force locates at the middle-bottom part of the pile. The bending moment is unidirectional positive. In addition, the bending moment increases with t increase in the bury depth, and the bending moment is the minimum at the pile top.

3.4.2 Shear Force and Bending Moment at the Anchored Segment

In the present article, the deep beam theory based on the m method is applied. Fig. 8 shows that model and the load conditions. The pile bottom is treated as a free end.

With the previous study, the shear force and the bending moment at the anchored segment are

$$Q(x)=\left(\frac{mb_p}{EI}\right)^{\frac{3}{5}}EI[x_0A_4+\frac{\theta_0}{\left(\frac{mb_p}{EI}\right)^{\frac{1}{5}}}B_4+\frac{M_0}{\left(\frac{mb_p}{EI}\right)^{\frac{2}{5}}EI}C_4+\frac{Q_0}{\left(\frac{mb_p}{EI}\right)^{\frac{3}{5}}EI}D_4], \tag{29}$$

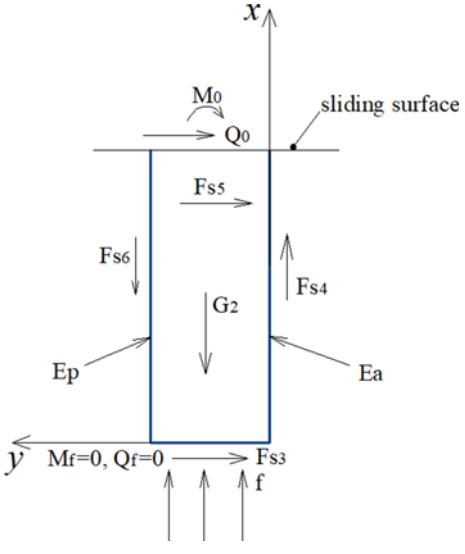

Fig. 8. Internal Force Calculation of the Anchored Segment (E_a, E_p, G_2, F_{s4} and F_{s6} are the active soil pressure, the passive soil pressure, the gravity load of the anchored segment, the friction force behind the anchored segment and the friction force ahead the pile, respectively.)

$$M(x)=\left(\frac{mb_p}{EI}\right)^{\frac{2}{5}}EI[x_0A_3+\frac{\theta_0}{\left(\frac{mb_p}{EI}\right)^{\frac{1}{5}}}B_3+\frac{M_0}{\left(\frac{mb_p}{EI}\right)^{\frac{2}{5}}EI}C_3+\frac{Q_0}{\left(\frac{mb_p}{EI}\right)^{\frac{3}{5}}EI}D_3], \tag{30}$$

where x_0, θ_0, Q_0 and M_0 are the displacement, the inclination angle, the shear force and the bending moment on the slide surface. A_i, B_i, C_i and D_i are the influential function value listed in the corresponding table.

Equations (29) and (30) show that the maximum values of the shear force and the bending moment locate at the bottom of the anchored segment. The minimum value of the shear force locates at the top and the bottom of the anchored segment. In addition, the variation of the shear force is more prominent than that of the bearing segment. Moreover, the bending moment is unidirectional positive and reaches the minimum values at the bottom and the top of the pile.

4. Case Study

4.1 Numerical Model and Design Parameters

To verify the above results, we established a numerical model based on the model in Fig. 1 (Fig. 9). The weight cohesion, internal friction angle of the soil were 18 kN/m^3, 26 kPa and 10^0, respectively. The foundation coefficient on the sliding surface and the corresponding proportionality coefficient were 4×10^3 kN/m^3 (k) and 2.6×10^3 kN /m^4 (m), respectively. The anti-slide pile consisted of the concrete and the steel bar. The compressive strength and the tensile strength of the concrete, graded C30, were 14.3 MPa and 1.43 MPa, respectively. The main steel bars were HRB 400 and no inclined steel bars were installed. The spacing and the protection thickness of the steel bar with the diameter and submit strength of 18 mm and 360 MPa were 140 mm and 70 mm. The width, thickness, length and the bearing length of the pile were 3 m, 2.5 m, 15 m and 9 m, respectively. To promote the shear strength of the pile, vertical structural steel bars with the spacing

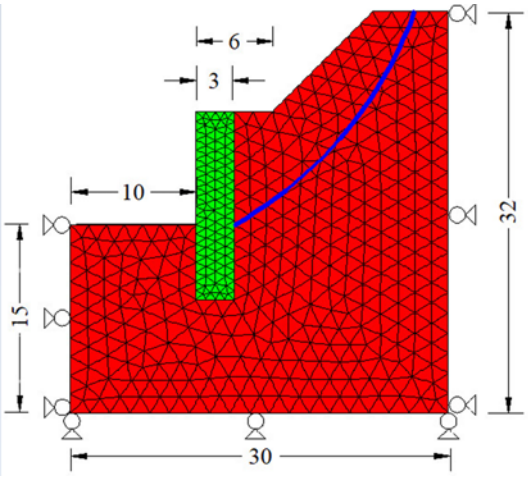

Fig. 9. Calculation Model (unit: m)

Table 1. Mechanical Parameters

Soil	Weight γ_s/kN/m^3	Elastic modulus E_s/MPa	Poison ratio υ_s	Side friction q_{s1}/kPa	Side friction q_{s2}/kPa	Anti-pile	Weight γ/kN/m^3	Elastic modulus E/GPa	Poison ratio υ
	18	21	0.37	30	38		26	22	0.25

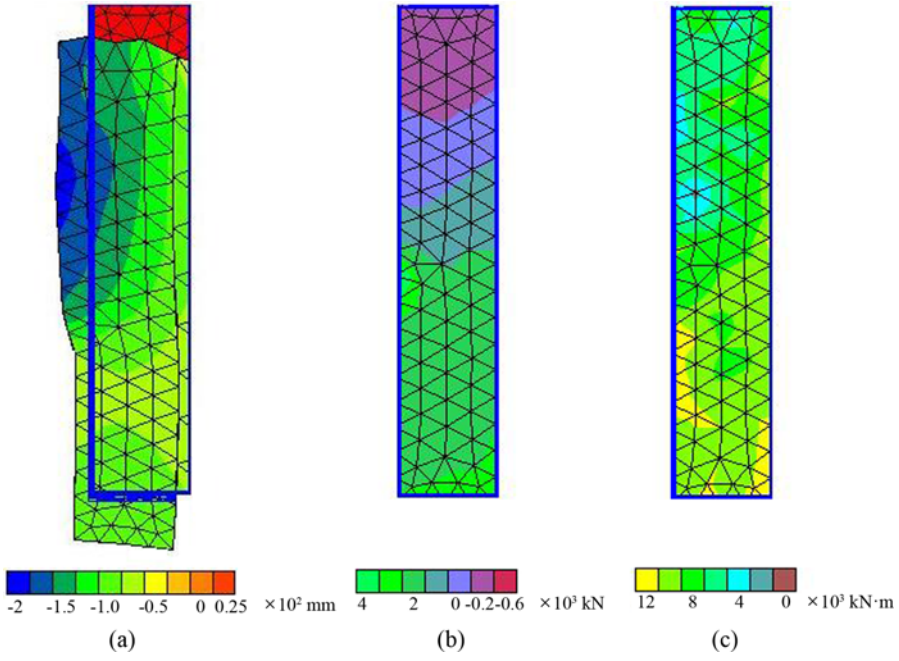

Fig. 10. Calculation Results by Numerical Calculation: (a) Displacement Distribution, (b) Shear Force Distribution, (c) Bending Distribution

of 300 mm were installed at the compression parts.

The numerical model, based on FLAC 3D and adopting tetrahedral elements, consisted of 8512 elements and 2153 grids. The soil and the beam consisted of brick and beam element, respectively. In addition, interface elements were installed on the soil-beam interface. To promote the calculation accuracy, the number of the beam grids was increased. In the calculation model, lateral displacement boundaries of the slope were set in the X and Y direction. At the bottom of the slope, the displacements in the X, Y and Z directions were restricted. The other surfaces of the slope were free.

In the model, the lateral and bottom surfaces are fixed. Table 1 lists the main mechanical parameters. Fig. 9 shows the calculation model and the corresponding grids.

4.2 Numerical Results

Figure 10 shows the horizontal displacement and the internal force of the anti-slide pile. The maximum displacement (negative) at the loaded segment is about 200 mm (Fig. 10(a)). When the distance between the bottom of the pile and the monitor point is 14 m, the horizontal displacement is zero. At the bottom, a positive displacement (25 mm) forms. Clearly, the displacement various at the loaded segment is more prominent. Fig. 10(b) shows that the maximum shear forces at the anchored segment and the loaded segment are 4,000 kN and 600 kN, respectively. In addition, the maximum shear force forms at the middle-bottom part of the anchored segment. For the bending moment, Fig. 10(c) indicates that the maximum bending moment (12,000 kN·m) forms at the middle-bottom part of the anchored segment.

4.3 Results Comparison

Figure 11(a) shows that the displacement in the preliminary shallow beam model is linear to the depth. The maximum value locates at the bottom, and the distance between the rotation center and the top is about 13 m. For the deep beam model, the pile displacement is nonlinear to the depth. Clearly, the displacements are lower than 0, thus, the rotation center fails to form in the pile. Especially, the variation rate of the displacement peaks on the slide surface. In addition, at the loaded segment, the displacement is lower than that obtained using the preliminary beam model, whereas the opposite occurs at the anchored segment.

In the preliminary shallow beam model, shear force is linearly to the depth at the loaded segment (Fig. 11(b)). At the anchored segment, a hump-shaped curve of the shear force forms. When the distances from the pile top are 9 m and 13 m, the absolute value of the shear force reaches two extreme values. When the distance is 10.4 m, the shear force is zero. In the deep beam model, the shear force at the anchored segment is similar to that in the preliminary beam model. The maximum error between these curves is 15%. However, the error at the loaded segment is larger despite of the similar locations for the maximum shear forces and the neutral points. In addition, these methods show that shear forces are the

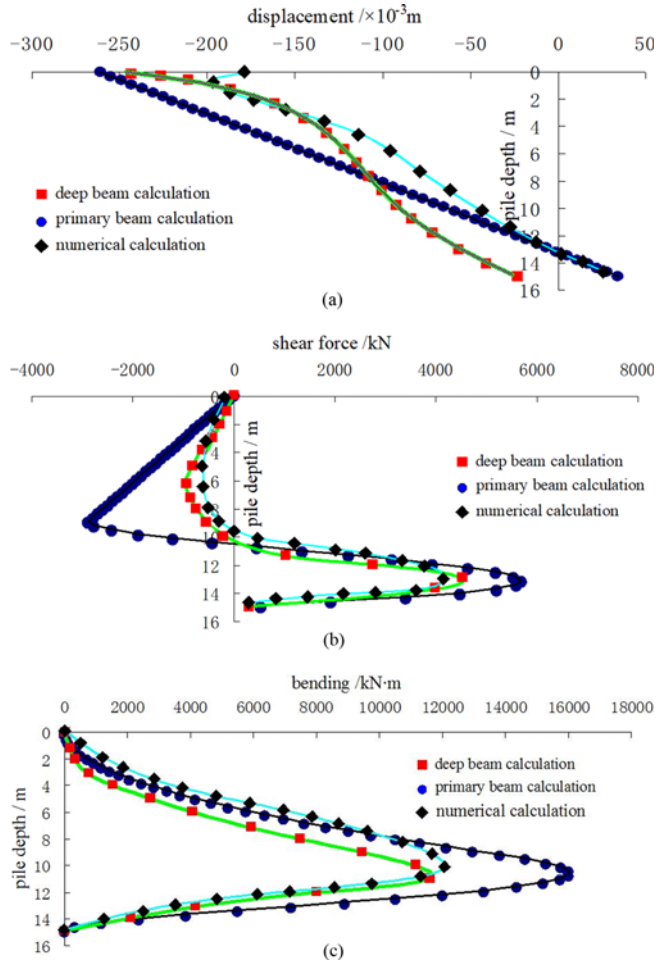

Fig. 11. Displacement and Internal Force Calculation: (a) Displacement Distribution, (b) Shear Force Distribution, (c) Bending Distribution

minimum at the top and bottom of the pile.

Figure 11(c) indicates that the curves of the positive bending moment obtained using two methods are hump-shaped, and the maximum values locate at the middle-bottom part of the pile (10.7 m). In addition, the maximum error between two curves is about 21%. Moreover, at the top and the bottom of the pile, the bending moments are zero.

The above results show that the displacement, the shear force and the bending moment, obtained using the preliminary shallow beam, are higher than those in the deep beam and numerical models. In addition, the results, obtained using the deep beam theory, agree well with the numerical results. This phenomenon may result from the weak boundary conditions and the ignorance of the friction force in the preliminary beam model. Additionally, in the deep beam model, the geometric size, the load conditions and the boundary conditions of the pile are proper. Thus, the reasonability of this method is properly verified.

5. Conclusions

1. According to the geometric sizes, the load distribution characteristics and the fact that the section deformation fails to meet the planar assumption, the concrete deep beam is more suitable to describe the anti-slide beam. Because shear failure, bending-shear failure and local failure are ignored by the shallow beam model.
2. According to the load distribution characteristics, we proposed a tie rod arch model with variable sections, consisting of the concrete (the inclined compressive bar at the bearing segment and the anchored segment) and the steel bar (the tension bar at the tension segment). in addition, the power function relation between shear span ratio and opposite inclination angle the tie rod arch indicates that the increase in shear span ratio results in the decrease in the inclination angle (with reducing decrease rate). The shear strength positively relates the variation in the arch curvature. The decrease in the shear span ratio results in the increase in the inclination angle of the tie rod arch (with elevating increase rate), whereas the variation in the curvature and the influence on the shear strength are minor.
3. The numerical study shows that in the shallow beam model, the displacement is linear to the depth for the free bottom boundary. However, in the deep beam model, the displacement is nonlinear to the depth with the maximum variation ratio at the sliding surface. The displacement in the deep beam model in which the rotation center is absent is smaller than the shallow beam model with the maximum value of 23%. In addition, for the shear stress, these two model yield close results with the maximum error of 15% at the anchored segment. Whereas for the bearing segment, the differences in results are larger. Nevertheless, these two methods agree that the maximum negative and positive shear stresses locate the sliding surface and the location which is 1/3 anchorage length higher than the bottom point. Moreover, for the bending moment is single-hump distributed without negative bending moment. The maximum value locates 2 m away from the sliding surface with a relative error of 21%.

Acknowledgments

The authors gratefully acknowledge the support from the Natural Science Foundation of Hunan Province (No.2019JJ40056), the National Natural Science Foundation of China (No.51804110), Scientific Research Foundation of Hunan Province Education Department (No.18A345, 18B391, 19B124), and the construct program of applied specialty disciplines in Hunan province. These works are gratefully acknowledged.

ORCID

Not Applicable

References

Brandenberg SJ, Boulanager RW, Kutter BL, Chang DD (2005) Behavior

of pile foundations in laterally spreading ground during centrifuge tests. *Journal of Geotechnical and Geoenvironmental Engineering* 131(11):1378-1391, DOI: 10.1061/(ASCE)1090-0241(2005)131:11(1378)

Dai ZH, Shen PS (2003) Improvements on calculation of internal forces of cantilever anti-sliding piles. *Journal of Hunan University (Natural Sciences)* 30(3):81-85, DOI: 10.3321/j.issn:1000-2472.2003.03.021 (in Chinese)

Fu QX, Zhang XM (1992) Investigation of reinforced concrete cantilever deep beams subjected to shear. *Journal of South China University of Technology (Natural Science)* 20(1):9-15 (in Chinese)

Kahyaoglu MR, Onal O, Imanchn G, Ozden G, Kayalar AS (2012) Soil arching and load transfer mechanism for slope stabilitied with piles. *Journal of Civil Engineering and Management* 18(5):701-708, DOI: 10.3846/13923730.2012.723353

Kourkoulis R, Gelagoti F, Anastasopoulos I, Gazetas G (2011) Slope stabilizing piles and pile group: Parametric study and design insights. *Journal of Geotechnical and Geoenvironmental Engineering* 137(7):663-677, DOI: 10.1061/(ASCE)GT.1943-5606.0000479

Lei GP, Tang HM, Li CD, Song DW, Cheng H, Wu Q (2013) Study ofimproved design method of anti-slide pile socketed segment. *Chinese Journal of Rock Mechanics and Engineering* 32(3):605-614, DOI: 10.3969/j.issn.1000-6915.2013.03.019 (in Chinese)

Li J, Jiang XG, Wang HZ, Luo S, Xia WZ, Li X (2018) Analytical element for Timoshenko beam on elastic foundation. *Engineering Mechancis* 35(2):221-229, DOI: 10.6052/j.issn.1000-4750.2016.10.0834 (in Chinese)

Li CD,Wu JJ, Tang HM, Wang J, Chen F, Liang DM (2015) A novel optimal plane arrangement of stabilizing piles based on soil arching effect and stability limit for 3D colluvial landslides. *Engineering Geology* 195:236-247, DOI: 10.1016/j.enggeo.2015.06.018

Liu J, Wang J (2018) The effect of indentation sequence on rock breakages: A study based on laboratory and numerical tests. *Comptes Rendus Mecanique* 346(1):26-38, DOI: 10.1016/j.crme.2017.11.004

Matsui T, San KC (1992) Finite element slope stability by shear strength reduction technique. *Soils and Foundations* 32(1):59-90

Wang YX, Guo PP, Ren WX, Yuan BX (2017) Laboratory investigation on strength characteristics of expansive soil treated with jute fiber reinforcement. *International Journal of Geomechanics* 17(11):04017101, DOI: 10.1061/(ASCE)GM.1943-5622.0000998

Wang LP, Zhang G (2014) Centrifuge model test study on pile reinforcement behavior of cohesive soil slopes under earthquake conditions. *Landslides* 11(2):213-223, DOI: 10.1007/s10346-013-0388-2

Xia GY, Li CX, Zeng QY (2010) Finite element formulation of Timoshenko beam on Winkler elastic foundation. *Journal of Central South University (Science and Technology)* 41(4):1549-1555 (in Chinese)

Xia GY, Zeng QY (2015) Timoshenko beam theory and its applications. *Mechanics in Engineering* 37(3):302-316, DOI: 10.6052/1000-0879-14-080 (in Chinese)

Xia GY, Zeng QY (2016) Analysis of nodal load distribution of crossed foundation beam based on the theory of Timoshenko beam on Winkler foundation. *Engineering Mechancis* 32(2):88-95 (in Chinese)

Xu RQ, Wu YF (2007) Static, dynamic, and buckling analysis of partial interaction composite members using Timoshenko's beam theory. *International Journal of Mechanical Sciences* 49:1139-1155, DOI: 10.1016/j.ijmecsci.2007.02.006

Yin J, Deng RG, Wang JM, Wang YY, Li KT (2017) Transfer matrix algorithm for calculating internal forces of andi-sliding pile with anchor cable. *Rock and Soil Mechanics* 38(12):3517-3531, DOI: 10.16285/j.rsm.2017.12.016 (in Chinese)

Zhao YL, Zhang LY, Wang WJ, Tang JZ, Lin H, Wan W (2017) Transient pulse test and morphological analysis of single rock fractures. *International Journal of Rock Mechanics & Mining Sciences* 91:139-154, DOI: 10.1016/j.ijrmms.2016.11.016

Zhao YL, Zhang LY, Wang WJ, Wan W, Ma W (2018) Separation of elastoviscoplastic strain of rock and a nonlinear creep model. *International Journal of Geomechanics* 18:04017129, DOI: 10.1061/(ASCE)GM.1943-5622.0001033